Journal of Medicinal Chemistry

Article

pubs.acs.org/jmc

Structural Basis for Inhibition of the Fat Mass and Obesity Associated Protein (FTO)

WeiShen Aik, Marina Demetriades, Muhammad K. K. Hamdan, Eleanor. A. L. Bagg, Kar Kheng Yeoh,† Clarisse Lejeune, Zhihong Zhang, Michael A. McDonough,* and Christopher J. Schofield*

Chemistry Research Laboratory, University of Oxford, 12 Mansfield Road, Oxford OX1 3TA, United Kingdom

Supporting Information

ABSTRACT: The fat mass and obesity associated protein (FTO) is a potential target for anti-obesity medicines. FTO is a 2-oxoglutarate (2OG)-dependent *N*-methyl nucleic acid demethylase that acts on substrates including 3-methylthymidine, 3-methyluracil, and 6-methyladenine. To identify FTO inhibitors, we screened a set of 2OG analogues and related compounds using differential scanning fluorometry- and liquid chromatography-based assays. The results revealed sets of both cyclic and acyclic 2OG analogues that are FTO inhibitors. Identified inhibitors include small molecules that have been used in clinical studies for the inhibition of other 2OG oxygenases. Crystallographic analyses reveal inhibition by 2OG cosubstrate or primary substrate competitors as well as compounds that bind across both cosubstrate and primary substrate binding sites. The results will aid the development of more potent and selective FTO inhibitors.

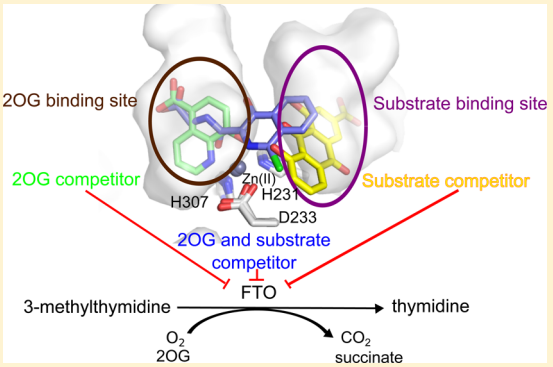

INTRODUCTION

There is an unmet medical need for new approaches to treating obesity. Mutations to the *fto* gene are associated with increased body mass, as shown by genome-wide association and mouse model studies.[1−3] The *fto* gene product, FTO, is an *N*-methyl nucleic acid demethylase acting on both single-stranded DNA and RNA substrates, including 3-methylthymine, 3-methyluracil, and 6-methyladenine (Scheme 1).[4−6] How the modulation of nucleic acid methylation status by FTO relates to increased body mass is unknown. Possible mechanisms include altered metabolism, appetite regulation, or both. Inhibition of FTO activity by small molecules has been proposed as a potential treatment for extreme obesity,[7] but validation of this approach requires the development of selective inhibitors.

Scheme 1. Reactions Catalyzed by FTO

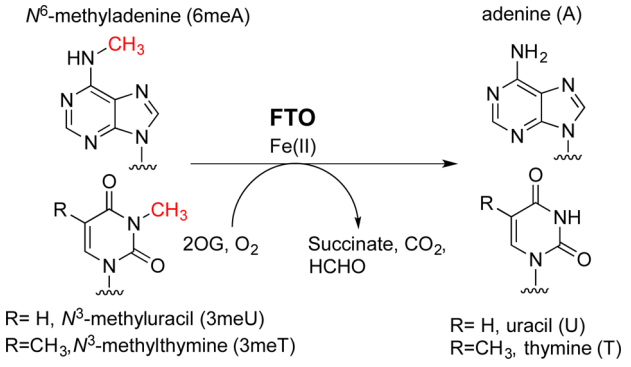

FTO is a member of the Fe(II) and 2-oxoglutarate (2OG)-dependent oxygenase family, of which there are >60 members predicted in humans. Human nucleic acid oxygenases (NAOXs) include the AlkB homologues (ABH 1−8), and the ten−eleven translocation enzymes (TETs 1−3). Some human NAOXs are known to have "biochemical roles" in DNA repair, RNA-hydroxylation, and 5-methylcytosine oxidation.[7−10] 2OG oxygenases are being targeted for therapeutic intervention. These include γ-butyrobetaine hydroxylase, the hypoxia-inducible transcription factor (HIF) prolyl- and asparaginyl-hydroxylases, and the N^{ε}-methyllysine histone demethylase (JmjC) enzymes.[11] However, there have been few reports on the inhibition of NAOXs.[12] Here, we report biochemical and crystallographic studies on FTO inhibition. The results will aid in the development of potent and selective inhibitors suitable for validation of FTO as an obesity target.

RESULTS

We initially employed a differential scanning fluorometry (DSF)-based assay to screen >150 2OG analogues and metal-chelators consisting of 10 structural series. Where the DSF assay was not suitable due to compound fluorescence (e.g., 8-hydroxyquinolines), we assayed FTO inhibition using liquid chromatography (LC). The LC assay was also used to determine IC_{50} values for hits. These studies led to the identification of structurally different FTO inhibitors, including the well-characterized 2OG oxygenase inhibitors *N*-oxalylgly-

Received: February 8, 2013

   dx.doi.org/10.1021/jm400193d | J. Med. Chem. XXXX, XXX, XXX−XXX

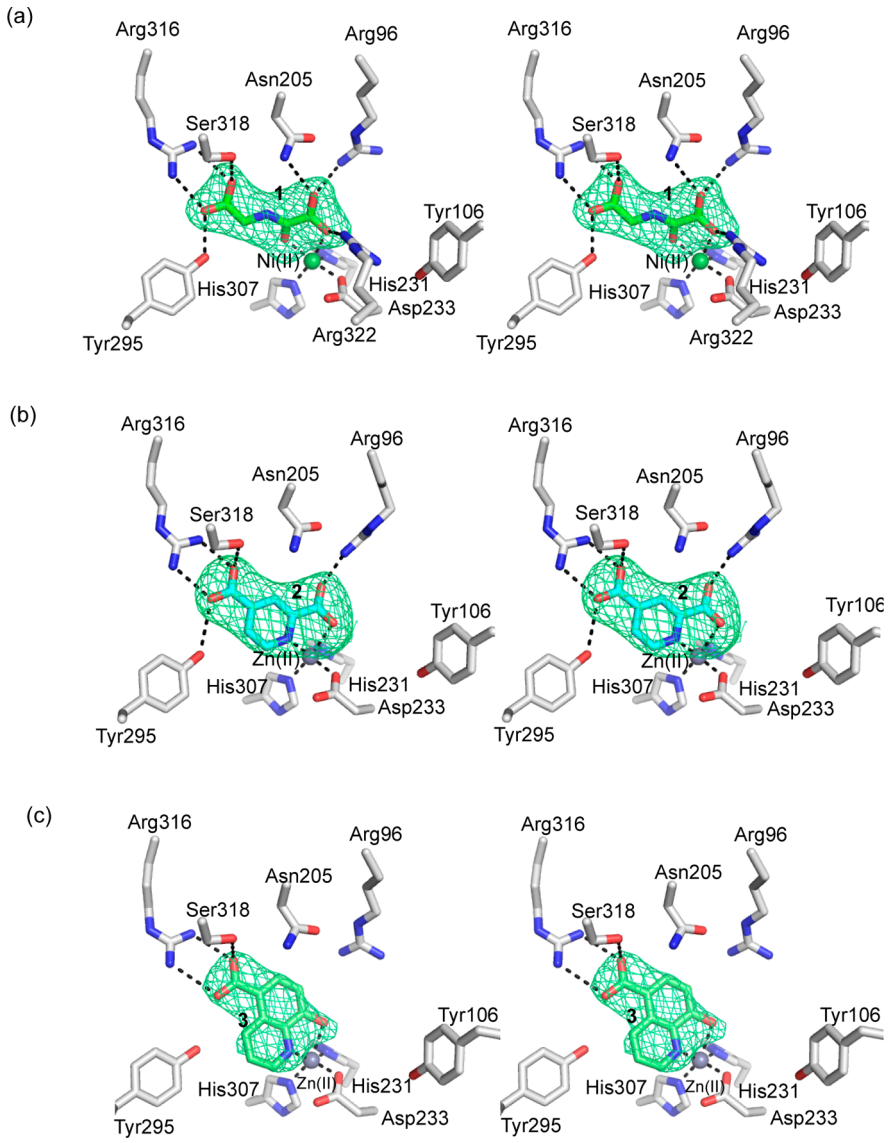

Figure 1. Wall-eyed stereo views from crystal structures of FTO in complex with (a) **1** (green), (b) **2** (cyan), and (c) **3** (light green). Residue side chains C (white), O (red), N (blue), Ni (green ball), Zn (gray ball), and hydrogen bonds are indicated as black dashes. mFo-DFc ligand omit maps (contour level, σ = 3.0) are indicated as lime green mesh.

cine and pyridine-2,4-dicarboxylate, as well as hydroxyquinoline-, pyridyl-, and isoquinoline-based compounds. We then performed structural studies with representatives of different classes of the identified inhibitors.

A crystal structure of FTO in complex with *N*-oxalylglycine (NOG) (a 2OG analogue) and 3-methylthymidine (3meT) has been reported.[13] Initially, we determined structures for FTO in complex with two broad-spectrum 2OG oxygenase inhibitors, NOG, **1**, (2.4 Å resolution) (Figure 1a) (PDB ID: 4IDZ) and pyridine-2,4-dicarboxylate, **2**, (2.5 Å resolution) (Figure 1b) (PDB ID: 4IE0). As observed for some of the JmjC demethylases,[14−16] **2** (IC_{50} 8.3 μM) was a more potent inhibitor than **1** (IC_{50} 44 μM, Table 1). Although the structures were obtained under different conditions (Ni and Zn substituting for Fe with **1** and **2**, respectively, and in the presence of N^6-methyladenosine for **1**), in each case, a molecule of glycerol (likely from the cryoprotectant) was observed in the previously identified 3meT substrate binding site (Supporting Information Figure S2a).[13] Consistent with observations of other 2OG oxygenase-inhibitor complexes, **1** and **2** are located in the 2OG binding pocket, with the C-5 carboxylate of **1** and C-4 carboxylate of **2** positioned to form electrostatic and hydrogen-bonding interactions with the side chains of Arg-316, Ser-318, and Tyr-295. Both **1** and **2** are positioned to chelate in a bidentate manner to the metal. In each case, the C-1 carboxylate is positioned trans to the His-307 imidazole and the other chelating group (amide carbonyl for **1**, and pyridyl nitrogen for **2**) trans to the Asp-233 carboxylate.

We also determined a structure (2.5 Å resolution) for FTO·Zn in complex with **3**[17] (Figure 1c) (PDB ID: 4IE4), a relatively potent FTO inhibitor (IC_{50} 3.3 μM), which also inhibits other 2OG oxygenases.[14] Two derivatives of **3**, in which the carboxylate was substituted with a sulfonamide, were less potent (IC_{50} 23 μM for **4** and 18 μM for **5**). The FTO·Zn·**3** structure reveals the C-5 carboxylate in a position similar to that observed for the side chain carboxylates of **1** and **2**, rationalizing the reduced potencies of the C-5 sulfonamides, **4** and **5**. In the FTO·Zn·**3** complex, the relative metal coordination positions of the hydroxyl and nitrogen of the hydroxyquinoline are swapped relative to the active site

dx.doi.org/10.1021/jm400193d | *J. Med. Chem.* XXXX, XXX, XXX−XXX

Table 1. Structures of Selected FTO Inhibitors from This Study and the Tm Shift Values (ΔTm/°C), Residual FTO Activity at 200 μM Compound Concentration (SPA/%), and IC_{50} Values for Hydroxyquinoline-, Pyridyl-, and Isoquinoline-Based Inhibitors[a]

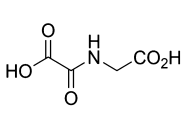

1 (44±1.1 μM)

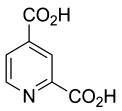

2 (8.3±1.1 μM)

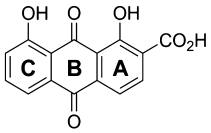

19 (9.0±1.1 μM)

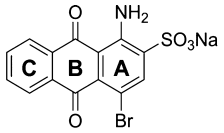

20 (11±1.1 μM)

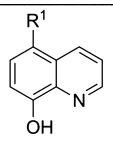

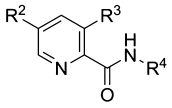

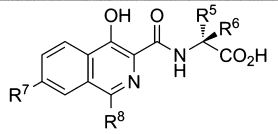

No.	R^1	R^2	R^3	R^4	ΔTm (°C)/ SPA (%)	IC_{50} (μM)	No.	R^5	R^6	R^7	R^8	ΔTm (°C) / SPA (%)	IC_{50} (μM)
3	CO_2H				NA	3.3±1.1	**11**	H	H	H	Cl	12 °C	2.8±0.9
4	SO_2NH_2				14%	23±1.2	**12**	CH_2Ph	H	H	Cl	28 °C	38±1.1
5	SO_2NHMe				17%	18±1.2	**13**	CH_3	H	H	Cl	26 °C	60±1.1
6		H	OH	CH_2CO_2H	25%	15±1.1	**14**	$CH_2(CH_3)_2$	H	H	Cl	23 °C	120±1.1
7			H		NA	120± 1.2	**15**	H	CH_2Ph	H	Cl	29 °C	84±1.1
8		H	OH	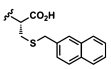	9 °C	92±1.2	**16**	H	CH_3	H	Cl	29 °C	110±1.1
9			OH	CH_2CO_2H	16%	96±1.2	**17**	H	$CH_2(CH_3)_2$	H	Cl	17 °C	160±1.1
10			OH	CH_2CO_2H	19%	43±1.2	**18**	H	H	OPh	Me	NA	9.8±1.1

[a]For compounds **1**, **2**, **19**, and **20**, IC_{50} values are in parentheses. Standard deviations were calculated from triplicate experiments.

HxD···H metal binding motif when compared with a JMJD2A·Ni·**3** structure[14] (JMJD2A is a histone demethylase). JMJD2A structures show a shift in the metal position upon **3** binding;[14] however, no such difference in metal position was observed for FTO.

The observed binding modes of **1** and **2** prompted the investigation of pyridyl glycinamides (Table 1; **6**,[12] **7**, **8**,[12] **9**,[18] and **10**[18]). Although these compounds were less potent than the parent templates, the results reveal that in this series, the presence of a C-3 hydroxy group increases potency, and substitution at the glycyl Cα position is possible (see Table 1). We determined a structure (2.0 Å resolution) of FTO·Zn in complex with **6** (Figure 2a) (PDB ID: 4IE5), which also inhibits the alkylated-DNA repair enzyme AlkB (*Escherichia coli*) (IC_{50} 3.4 μM).[12] A structure of the AlkB·Fe·**6** complex reveals **6** bound in the 2OG binding site with its pyridine ring positioned in a hydrophobic pocket buried within the core of the double-stranded β helix (DSBH) fold (Supporting Information Figure S2c),[12] leading to the prediction that **6** may bind similarly to FTO without disrupting nucleotide binding.[19] To our surprise, the FTO·Zn·**6** complex shows that **6** binds to FTO differently from that observed in AlkB. In both FTO and AlkB, the side chain carboxylate of **6** is positioned to bind in the 2OG pocket; however, the hydrophobic pocket of AlkB in which the pyridine ring of **6** binds is apparently larger; more flexible; and, thus, more accommodating than that of FTO. As a result, the pyridine ring of **6** is positioned closer to the substrate binding site in FTO. Superimposition of the FTO·Zn·**6** and FTO·Fe·NOG·3meT structures (Supporting Information Figure S2b) shows that the C5 of the pyridine ring of **6** is positioned ∼1.4 Å from the 3meT carbonyl oxygen, suggesting that **6** may sterically hinder binding of FTO's nucleic acid primary substrate.

Compound **11** (FG-2216/IOX3)[20] is a known inhibitor of the HIF-prolyl hydroxylases (PHD1−3) that is active in cells and animals.[11] It gave the lowest IC_{50} value against FTO (2.8 μM). Substitution of the glycine side chain[21] of **11** led to reduced potency; however, the D-amino acid derivatives (D-phenylalanine, **12**, IC_{50} 38 μM; D-alanine **13**, IC_{50} 60 μM; D-valine, **14**, IC_{50} 120 μM) were generally more potent than the L-derivatives (L-phenylalanine, **15**, IC_{50} 84 μM; L-alanine, **16**, IC_{50} 110 μM; L-valine, **17**, IC_{50} 160 μM). Notably, a previous study shows that **13** is relatively less active than **16** against PHD2,[22] suggesting that selectivity for FTO over PHD2 may be achieved using the isoquinoline scaffold. Moreover, the PHD inhibitor **18** (FG-4592 as identified by SelleckBio),[21] displayed relatively potent FTO inhibition (IC_{50} 9.8 μM).

A crystal structure of FTO in complex with **11** was determined (2.50 Å resolution) (Figure 2b) (PDB ID: 4IE6) and shows **11** binds FTO similarly to **6**. The chlorine of **11** sits in the nucleic acid substrate binding site. An unusual metal coordination geometry was observed for **11**; the side chain amide carbonyl deviates from planarity with respect to the isoquinoline ring by ∼60°, making the isoquinoline ring nitrogen-to-metal coordination skewed. This may be due to the position of the side chain of Arg-96 with respect to the bicyclic rings, sterically forcing a non-ideal metal coordination by the compound.

A recent study has identified the natural product rhein as a reversible and competitive FTO inhibitor and led to the prediction that rhein (**19**) binds to the 2OG, Fe(II), and 3meT binding sites, also interacting with Arg-316.[19] Consistent with the reported work, we found that **19** is an FTO inhibitor, with

dx.doi.org/10.1021/jm400193d | J. Med. Chem. XXXX, XXX, XXX−XXX

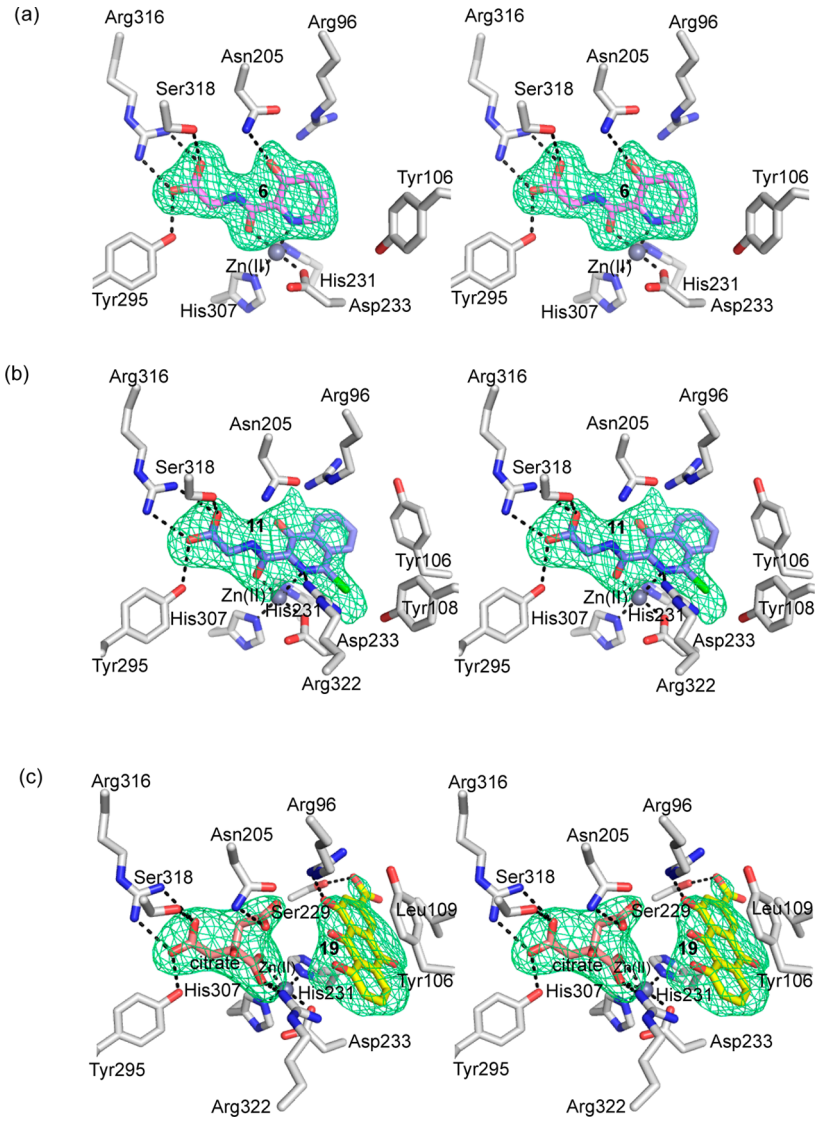

Figure 2. Wall-eyed stereo views from crystal structures of FTO in complex with (a) **6** (pink); (b) **11** (blue), Cl (green); (c) **19** (yellow), and citrate (light red). Labeling and color as in Figure 1.

an IC_{50} of 9.0 μM. Compound **20** was found to be similarly potent (IC_{50} 11 μM) despite its different substitution pattern. We determined a structure of the FTO·Zn·**19** complex (2.6 Å resolution) (Figure 2c and Supporting Information Figure S2d) (PDB ID: 4IE7). Under our crystallization conditions, **19** is observed bound to the nucleic acid substrate binding site, as opposed to the predicted 2OG binding site. The C-2 carboxylate of **19** is positioned to hydrogen bond with the Ser-229 side chain OH (2.7 Å). The A-ring of **19** is positioned to form partial $\pi-\pi$ interactions with His-231 and forms a hydrogen bond between the 4-hydroxyl group of the A-ring and the side chain of Arg-96.

A citrate molecule from the crystallization buffer is observed in the 2OG binding site in the FTO·**19** structure. One of the citrate carboxylates is positioned to interact with the active site metal, similar to succinate binding observed in other 2OG oxygenase structures,[23] and another carboxylate is interacting with the side chain of Arg-316. The third citrate carboxylate is positioned to hydrogen-bond to the side chain of Asn-205. The IC_{50} for citrate was found to be 300 μM; fumarate (IC_{50} 150 μM) and L-2-hydroxyglutarate (IC_{50} 320 μM) were also shown to inhibit FTO weakly (Supporting Information Table S1). Although these values are relatively high, given the links of FTO to obesity, it raises the possibility that FTO inhibition by endogenous small molecules (e.g., tricarboxylic acid (TCA) cycle intermediates and related compounds such as L-2-hydroxyglutarate) may be of physiological or pathophysiological relevance, as proposed to occur for other 2OG oxygenases.[15,24] IC_{50} values for FTO inhibition by other TCA cycle intermediates were all >1 mM.

DISCUSSION AND CONCLUSIONS

Overall, we have identified inhibitor templates that will provide starting points for the development of selective inhibitors to probe the physiological role of FTO-mediated nucleic acid demethylation. Most of the inhibitors investigated in this study utilize a metal chelating group for enhanced binding affinity and are 2OG competitors. Work with other 2OG oxygenases has shown that optimization of such compounds can lead to highly potent and selective inhibitors.[11] The structural analyses with compound **19** imply that efficient inhibition via substrate competition should also be possible. The results with the

dx.doi.org/10.1021/jm400193d | J. Med. Chem. XXXX, XXX, XXX−XXX

broad-spectrum inhibitors are important because they suggest that some of the previously observed biological effects of these compounds may be in part mediated via FTO (or other NAOX) inhibition. A cell-penetrating form of **1**[25] has been widely used as a hypoxia mimic.[11,26] It may be that some of the observed effects of **1** are due to the inhibition of 2OG oxygenases other than the HIF hydroxylases. Notably, among the most potent FTO inhibitors we identified, compounds **11** and **18** are in clinical trials as prolyl-hydroxylase inhibitors. Thus, the potential for FTO- and other 2OG oxygenase-mediated inhibition should be considered, and care should be taken when interpreting the physiological effects of these inhibitors.

EXPERIMENTAL SECTION

Purification of hFTO and hFTOΔ31. Protein purification methods were modified from methods previously reported for full length mouse FTO.[4] *E. coli* BL21 (DE3) transformed with the pET28a_hFTO plasmid (encoding for *N*-terminally hexahistidine-tagged full-length human FTO without the thrombin cleavage site between the hexahistidine tag and the protein) or pET28a_hFTOΔ31 (encoding for *N*-terminally hexahistidine-tagged human FTO with residues 2−31 deleted from the N terminus) were grown (37 °C; 180 rpm) to an OD_{600} of 0.6. FTO production was induced by the addition of 0.5 mM isopropyl β-D-1-thiogalactopyranoside (IPTG), and growth was continued at 16 °C for 16 h (hFTO) or 18 °C for 8 h (hFTOΔ31). The resultant cell pellets were stored at −80 °C. The cell pellets were thawed and resuspended in 20 mM Tris−HCl, pH 7.5; 500 mM NaCl; and 10 mM imidazole, then lysed by sonication on ice. The lysate was cleared by centrifugation, and the supernatant was loaded onto a 5 mL HisTrap FF column (GE Healthcare) and purified using an AKTA FPLC system. The column was treated with 20 mM Tris−HCl, 500 mM NaCl, and 40 mM imidazole, then eluted with 20 mM Tris−HCl, pH 7.5; 500 mM NaCl; and 500 mM imidazole. The eluted hFTOΔ31 protein solution was then treated with 200 mM EDTA. hFTOΔ31 was further purified using a (5 mL) HiTrap Heparin column (GE Healthcare) followed by a (20 mL) MonoQ column; in both cases, a gradient of buffer A (25 mM Tris−HCl, pH 7.5) and 50% buffer B (25 mM Tris−HCl, pH 7.5; 1 M NaCl) was used. Both proteins were then buffer-exchanged into 25 mM Tris−HCl, pH 7.5, and concentrated to 20 mg/mL for storage.

Dynamic Scanning Fluorometry Assays.[27] For dynamic scanning fluorometry (DSF) assays, a mixture (50 μL) containing 2 μM full-length FTO protein; 1× SYPRO orange dye (Invitrogen) (from commercial stock that is 5000×); 50 μM diammonium iron(II) sulfate complex; 200 μM test compound (or 2% DMSO control); and 50 mM HEPES, pH 7.5, was prepared. Assays were performed using a MiniOpticon Real-Time PCR Detection System (Bio-Rad). The sample plate was inserted into the machine, and fluorescence readings were taken between 25 and 90 °C, increasing the temperature linearly over 1 h 20 min. The excitation and emission wavelengths were 470 and 570 nm, respectively. Melting curves were analyzed using GraphPad Prism.

In Vitro Demethylation Assay. For catalytic assays, a 50 μL reaction mixture containing final concentrations of 3 μM FTO; 70 μM 3meT nucleoside; 160 μM 2OG; 500 μM L-ascorbate; 100 μM diammonium iron(II) sulfate complex; 200 μM test compound (2% DMSO in control reaction); and 50 mM 2-(*N*-morpholino)ethanesulfonic acid (MES), pH 6.3, was incubated at room temperature for 1 h. The reaction was quenched with methanol (50 μL) then centrifuged to remove precipitated protein. The supernatant was then dried using an Eppendorf Speedvac concentrator and reconstituted with (50 μL) water. The product (thymidine) and substrate (3meT) were separated using a Waters Acquity Ultra Performance Liquid Chromatography (UPLC) BEH C18 column (130 Å, 1.7 μm, 2.1 mm × 50 mm) with a gradient of 95% A (H_2O with 1% formic acid) to 80% B (methanol with 0.1% formic acid) over 5 min. The UV detection wavelength was set to 266 nm room temperature (thymidine) = 0.95 min, room temperature (3meT) = 1.48 min. (The liquid chromatography method was modified from that previously reported.[13]) The peaks were identified using a positive ion mode in the ESI-TOF mass spectrometry (Waters LCT Premier XE machine). The UV peaks were integrated using MassLynx software (Agilent), and the percentage conversion of 3meT to thymidine was used to quantify the activity of FTO in the presence of inhibitors. For IC_{50} determinations, assays were carried out in triplicate with a range of compound concentrations (0, 10, 30, 100, and 300 μM and 1, 3, and 10 mM). IC_{50} values were calculated from dose−response curves plotted using GraphPad Prism 5.

Protein Crystallization and X-ray Crystallography. Crystals of the hFTOΔ31 in complex with **1**, **2**, **3**, **6**, **11**, or **19** were grown in hanging drops at 293 K by the vapor diffusion method using 24 well pregreased VDX plates and round plastic coverslips (HR8-082, Hampton Research). The protein solution and reservoir solution (200 μL) conditions are listed in Table 2 (see below). Hanging drops were set up by adding protein solution to reservoir solution at a 2:1 ratio (total volume, 3 uL). The resultant crystals were cryoprotected using the well solution diluted with 15−20% v/v glycerol (cryoprotectant solution for the FTO·**19** crystal contains 1 mM **19**) then flash cooled in liquid nitrogen. Data were collected at 100 K for single crystals of FTO·**1**, FTO·**3**, and FTO·**6** complexes using a Rigaku FR-E+ Superbright copper rotating anode diffractometer equipped with an osmic HF optics, and a Saturn 944+ CCD detector. Data were collected at 100 K for FTO·**2**, FTO·**11**, and FTO·**19** using a single crystal at Diamond Beamline I03 equipped with a Pilatus 6M-F detector.

All data were indexed, integrated, and scaled using HKL2000.[28] The structures were solved by molecular replacement using the MR-PHASER[29] subroutine in PHENIX[30] using FTO:Fe:NOG:3meT (PDB ID: 3LFM) as a search model. Iterative cycles of model building and refinement were performed using COOT[31] and PHENIX until decreasing R and R_{free} no longer converged. A data collection and refinement statistics table can be found in Supporting Information Table S2.

Organic Synthesis Procedures. *General Information.* Reagents and solvents were from Aldrich, Alfa Aesar, or Acros. Compounds **1** and **2** were from Sigma Aldrich. Compounds **3**,[17] **6**,[12] **8**,[12] **9**,[18] **10**,[18] **11**,[20] and (**13**, **14**, **16**, **17**)[21,22] were prepared as described. Compound **18** was from Selleckbio, compounds **19** and **20** were from TCI UK, and 1-chloro-4-hydroxyisoquinoline-3-carboxylic acid was from Reddy Chemtech. Reactions were monitored by TLC, which was performed on precoated aluminum-backed plates (Merck, silica 60 F254). Flash column chromatography was carried out using a Biotage SP1 Purification system. Melting points were determined using a Leica Galen III hot-stage melting point apparatus and microscope. Infrared spectra were recorded from KBr discs, on

dx.doi.org/10.1021/jm400193d | J. Med. Chem. XXXX, XXX, XXX−XXX

Table 2. Crystallization Conditions for Protein and Reservoir Solutions[a]

	FTO·1	FTO·2		FTO·3		FTO·6		FTO·11		FTO·19	
PDB ID	4IDZ	4IE0		4IE4		4IE5		4IE6		4IE7	
protein solution conditions	~8 mg/mL hFTOΔ31, 1 mM $NiCl_2$, 3 mM **1**, 5 mM 6meA	~8 mg/mL hFTOΔ31, 1 mM $ZnSO_4$, 1 mM **2**		~8 mg/mL hFTOΔ31, 1 mM $ZnSO_4$, 2 mM **3**		~8 mg/mL hFTOΔ31, 1 mM $ZnSO_4$, 1 mM **6**		~8 mg/mL hFTOΔ31, 1 mM $ZnSO_4$, 1.5 mM **11**		~8 mg/mL hFTOΔ31, 1 mM $ZnSO_4$, 2 mM **19**	
reservoir solution conditions	85 mM trisodium citrate, pH 5.6; 14% PEG3350; 10% glycerol	100 mM trisodium citrate, pH 5.6; 11% PEG3350; 4% *tert*-butyl alcohol		100 mM trisodium citrate, pH 5.6; 13% PEG3350; 4% *tert*-butyl alcohol		100 mM trisodium citrate, pH 5.6; 9% PEG3350; 4% *tert*-butyl alcohol		100 mM trisodium citrate, pH 5.6; 11.5% PEG3350; 4% *tert*-butyl alcohol		100 mM trisodium citrate, pH 5.6; 11.5% PEG3350; 4% *tert*-butyl alcohol	

[a] 6meA: N^6-methyladenosine PEG3350/polyethylene glycol 3350.

a Bruker Tensor 27 FT-IR spectrometer. NMR spectra were acquired using a Bruker Avance II 500 MHz spectrometer equipped with a 5 mm $^{13}C(^1H)$ dual cryoprobe or Avance 400 MHz spectrometer equipped with a 5 mm *z*-gradient $^1H/^{13}C/^{19}F/^{31}P$ quadnucleus probe. Chemical shifts (δ) are given in parts per million, and the multiplicities are given as singlet (s), doublet (d), doublet doublet (dd), triplet (t), quartet (q), multiplet (m), or broad (br). Coupling constants, *J*, are given in hertz (±0.5 Hz). High resolution mass spectra (HRMS) were recorded using a Bruker MicroTOF. The purities of all compounds synthesized were ≥98%, as determined by analytical reverse-phase LC/MS or elemental analysis.

General Procedures. General Procedure A. A mixture of 8-hydroxyquinoline-5-sulfonic acid (2.4 g, 10 mmol) and chlorosulfonic acid (8 mL, excess) was stirred at room temperature overnight. The reaction was poured into ice water, and the formed yellow precipitate was filtered off and dried to obtain the desired sulfonyl chloride derivative (2.3g, 95%), which was kept under nitrogen at −20 °C.

To a solution of 8-hydroxyquinoline-5-sulfonic chloride (0.21 mmol, 50 mg) in acetonitrile (1 mL), the appropriate amine was added (1.05 mmol), and the reaction mixture was heated in a sealed tube. After evaporation in vacuo of the solvent, the mixture was dissolved in methanol, and the resulting crude product was purified using semipreparative reverse-phase HPLC performed on a Waters Sunfire C18 column (150 mm × 10 mm, 5 mm). Separation was achieved using a gradient of 0% B over 2 min and 0−50% B over 30 min, solvent A eluting at a flow rate of 5 mL/min, and monitoring at 254 nm. Solvent A: water +0.1% CF_3CO_2H. Solvent B: acetonitrile +0.1% CF_3CO_2H.

General Procedure B. To a solution of phenylalanine methyl ester hydrochloride (151 mg, 0.7 mmol, 1.2 equiv) and triethylamine (0.2 mL, 1.5 mmol, 2.5 equiv) in CH_2Cl_2 (10 mL) was added 1-chloro-4-hydroxyisoquinoline-3-carboxylic acid (130 mg, 0.6 mmol, 1 equiv), followed by benzotriazol-1-yl-oxytripyrrolidinophosphonium hexafluorophosphate (332 mg, 0.6 mmol, 1.1 equiv). The resulting mixture was then stirred at room temperature until completion (TLC). After 20 h, the organic solvents were removed, and the residue was purified by flash chromatography (hexane/EtOAc, 4:1) to afford the desired methyl-2-(1-chloro-4-hydroxyisoquinoline-3-carboxamido)propanoate derivative.

General Procedure C. A mixture of the methyl-2-(1-chloro-4-hydroxyisoquinoline-3-carboxamido)propanoate (110 mg, 0.3 mmol) in 1 N NaOH/MeOH (1:1) (10 mL, excess) was stirred at room temperature. TLC analysis (hexane/EtOAc, 4:1) indicated complete consumption of the starting material (R_f = 0.4) after 2 h. The reaction mixture was then washed with EtOAc (3 × 10 mL). The aqueous layer was acidified to pH 1 with 1 N HCl and then extracted with EtOAc (3 × 10 mL), dried ($MgSO_4$), filtered, and concentrated in vacuo to give the corresponding 2-(1-chloro-4-hydroxyisoquinoline-3-carboxamido)-3-phenylpropanoic acid derivative.

***N*-3-Methylthymidine.** The synthesis was modified from the previously reported method.[32] To a solution of thymidine (0.79 g, 3.26 mmol) and potassium carbonate (0.83 g, 6.01 mmol) in MeOH (50 mL), methyl iodide (0.38 mL, 6.1 mmol) was added dropwise at room temperature. The reaction was heated at 37 °C for 24 h, then 5 mL of acetic acid was added to neutralize the mixture. The solvent was evaporated in vacuo, and the crude compound was redissolved in water. The product

dx.doi.org/10.1021/jm400193d | J. Med. Chem. XXXX, XXX, XXX−XXX

was purified using preparative reversed-phase HPLC (t_R = 25 min) (Vydac 218TP C18, 250 mm × 22 mm, 10−15 μm, Grace Davison, USA) using a gradient of 2% B for 5 min, 2−98% B in A over 30 min, and 98% B for 5 min. Solvent A: 0.1% formic acid v/v water. Solvent B: 0.1% formic acid v/v in acetonitrile. Product (24%) mp 129−133 °C; IR (neat) ν/cm^{-1} 3500 (OH), 3412 (OH), 3300 (OH), 1683 (C═O), 1665 (C═O), 1622 (C═O); ^{1}H NMR (400 MHz, DMSO) δ 7.77 (1H, s, 6-H), 6.20 (1H, t, J = 6.5, 1′-H), 5.04 (1H, br. s, 5′-OH), 4.24 (1H, m, 3′-H), 3.78 (1H, app. q., J = 4.0, 4′-H), 3.58 (2H, m, 5′-H), 3.16 (3H, s, N−CH$_3$), 2.09 (2H, m, 2′-H), 1.82 (3H, s, CH$_3$); ^{13}C NMR (400 MHz, DMSO) δ 162.9 (*C*═O), 150.6 (*C*═O), 134.5 (6*C*), 108.3 (5*C*), 87.4 (4′*C*), 84.9 (1′*C*), 70.3 (3′*C*), 61.2 (5′*C*), 27.5 (N−CH$_3$), 13.0 (CH$_3$). HRMS calcd for $C_{11}H_{16}N_2NaO_5$ [M + Na]$^+$ 279.0951; Found 279.0951.

8-Hydroxyquinoline-5-sulfonamide (4). Following general procedure A, the reaction mixture was heated at 45 °C for 1 h. Compound **4** was isolated as a pale yellow solid (36.7 mg, 78%), mp dec 250 °C. t_R = 6.12; IR (neat) ν/cm^{-1} 3345, 3097, 2942, 2832, 1427, 1171, 1021; ^{1}H NMR (500 MHz, CD$_3$OD) δ 9.20 (1H, d, J = 9.0, Ar C*H*), 8.86 (1H, d, J = 4.5, Ar C*H*), 8.11 (1H, d, J = 8.0, Ar C*H*), 7.64 (1H, dd, J = 9.0, 4.0, Ar C*H*), 7.09 (1H, d, J = 8.0, Ar C*H*); ^{13}C NMR (500 MHz, CD$_3$OD) δ 155.6, 148.3, 138.8, 135.8, 131.7, 127.7, 125.8, 122.3, 108.7. HRMS calcd for $C_9H_8NO_4S$ (corresponding sulfonic acid)$^+$ 226.0169; Found 226.0161.

8-Hydroxy-*N*-methylquinoline-5-sulfonamide (5). Following general procedure A, the reaction mixture was heated at 70 °C for 2 h. Compound **5** was isolated as a pale yellow solid (35.5 mg, 71%), mp dec 190 °C. t_R = 5.89 min; IR (neat) ν/cm^{-1} 3346, 2943, 2832, 1152, 1021; ^{1}H NMR (500 MHz, CD$_3$OD) δ 9.18 (1H, dd, J = 8.5, 1.5, Ar C*H*), 8.84 (1H, br s, Ar C*H*), 8.10 (1H, d, J = 8.0, Ar C*H*), 7.61 (1H, dd, J = 8.5, 4.0, Ar C*H*), 7.08 (1H, d, J = 8.0, Ar C*H*), 2.54 (3H, s); ^{13}C NMR (500 MHz, CD$_3$OD) δ 155.9, 148.3, 139.0, 135.6, 131.5, 127.7, 125.8, 122.3, 108.6, 24.5 (CH$_3$). HRMS calcd for $C_9H_8NO_4S$ (corresponding sulfonic acid)$^+$ 226.0169; Found 226.0161.

(*R*)-2-(1-Chloro-4-hydroxyisoquinoline-3-carboxamido)-3-phenylpropanoate (25). Following general procedure B, **25** (147 mg, 66%) was isolated as a yellow oil (hexane/EtOAc, 4:1 R_f = 0.4); $[\alpha]_D^{22}$ −16.8 (*c*, 1.0 in CH_2Cl_2); IR (KBr) ν/cm^{-1} 3384 (N−H), 2925 (C−H), 1745 (HNC═O), 1638 (MeOC═O); ^{1}H NMR (500 MHz, CDCl$_3$) δ 12.85 (1H, s, ArOH), 8.34−8.37 (1H, m, Ar−*H*), 8.23−8.26 (1H, m, Ar−*H*), 8.21 (1H, d, J = 8.0, N*H*), 7.77−7.81 (2H, m, 2 × Ar−*H*), 7.23−7.34 (5H, m, 5 × Ph-*H*), 5.02−5.06 (1H, m, C*H*), 3.77 (3H, s, C*H*$_3$O), 3.31 (1H, dd, J = 14.0, 6.0, PhC*H*$_2$), 3.25 (1H, dd, J = 14.0, 7.0, PhC*H*$_2$); ^{13}C NMR (125 MHz, CDCl$_3$) δ 171.0 (*C*═O), 168.2 (*C*═O), 154.5 (Ar*C*), 139.3 (Ar*C*), 135.9 (Ph*C*), 130.5 (2 × PhCH), 130.0 (Ar*C*), 129.1 (Ar*C*), 128.9 (2 × PhCH), 128.5 (2 × ArCH), 127.0 (PhCH), 126.1 (ArCH), 123.1 (ArCH), 120.4 (Ar*C*), 52.9 (*C*H), 52.2 (*C*H$_3$O), 37.9 (PhCH$_2$). HMRS calcd for $C_{20}H_{16}ClN_2O_4$ [M − H]$^-$ 383.0804; Found 383.0805.

(*S*)-2-(1-Chloro-4-hydroxyisoquinoline-3-carboxamido)-3-phenylpropanoic Acid (26). Following general procedure B, **26** (130 mg, 59%) was isolated as a yellow oil (hexane/EtOAc, 4:1 R_f = 0.4); $[\alpha]_D^{22}$+17.5 (*c*, 1.0 in CH_2Cl_2); IR (KBr) ν/cm^{-1} 3384 (N−H), 2925 (C−H), 1745 (NC═O), 1639 (MeOC═O); ^{1}H NMR (500 MHz, CDCl$_3$) δ 12.86 (1H, s, ArO*H*), 8.35−8.37 (1H, m, Ar-*H*), 8.25−8.26 (1H, m, Ar-*H*), 8.21 (1H, d, J = 8.0, N*H*), 7.77−7.81 (2H, m, 2 × Ar-*H*), 7.23−7.34 (5H, m, 5 × Ph-*H*), 5.02−5.06 (1H, m, C*H*), 3.77 (3H, s, C*H*$_3$O), 3.31 (1H, dd, J = 14.0, 6.0, PhC*H*$_2$), 3.25 (1H, dd, J = 14.0, 7.0, PhC*H*$_2$); ^{13}C NMR (125 MHz, CDCl$_3$) δ 171.1 (*C*═O), 168.2 (*C*═O), 154.5 (Ar*C*), 139.3 (Ar*C*), 135.4 (Ph*C*), 130.5 (2 × PhCH), 130.0 (Ar*C*), 129.2 (Ar*C*), 128.9 (2 × PhCH), 127.0 (PhCH), 126.2 (ArCH), 123.1 (ArCH), 120.1 (Ar*C*), 52.9 (*C*H), 52.2 (*C*H$_3$O), 38.0 (PhCH$_2$). HMRS calcd for $C_{20}H_{16}ClN_2O_4$ [M − H]$^-$ 383.0804; Found 383.0804.

(*R*)-2-(1-Chloro-4-hydroxyisoquinoline-3-carboxamido)-3-phenylpropanoic Acid (12). Following general procedure C, **12** (100 mg, 95%) was isolated as a pale yellow solid; mp 184−186 °C; $[\alpha]_D^{22}$ −13.0 (*c*, 1.0 in MeOH); IR (KBr) ν/cm^{-1} 3448 (OH), 3362 (NH), 2930 (C−H), 1736 (NC═O), 1637 (HOC═O); ^{1}H NMR (500 MHz, DMSO-d_6) δ 13.49 (1H, s, ArO*H*), 8.93 (1H, d, J = 8.0, N*H*), 8.29−8.27 (1H, m, Ar-*H*), 8.22−8.24 (1H, m, Ar-*H*), 7.93−7.96 (2H, m, 2 × Ar-*H*), 7.26−7.27 (4H, m, 4 × Ph-*H*), 7.16−7.20 (1H, m, Ph-*H*), 4.79−4.84 (1H, m, C*H*), 3.28−3.33 (2H, m, PhC*H*$_2$); ^{13}C NMR (125 MHz, DMSO-d_6) δ 172.1 (C═O), 168.4 (*C*═O), 154.3 (Ar*C*), 138.5 (Ar*C*), 137.5 (Ph*C*), 131.8 (PhCH), 131.7 (PhCH), 129.4 (Ar*C*), 129.1 (2 × ArCH), 128.6 (Ar*C*), 128.3 (2 × PhCH), 126.6 (PhCH), 126.1 (ArCH), 123.0 (ArCH), 120.3 (Ar*C*), 53.2 (*C*H), 35.9 (PhCH$_2$). HMRS calcd for $C_{19}H_{14}ClN_2O_4$ [M − H]$^-$ 369.0648; Found 369.0651. Anal. ($C_{19}H_{15}ClN_2O_4$) requires: C, 61.55; H, 4.08; N, 7.56%; found C, 61.45; H, 4.00; N, 7.63%.

(*S*)-2-(1-Chloro-4-hydroxyisoquinoline-3-carboxamido)-3-phenylpropanoic Acid (15). Following general procedure C, **15** (90 mg, 92%) was isolated as a pale yellow solid; mp 185−188 °C; $[\alpha]_D^{22}$ +12.9 (*c*, 1.0 in MeOH); IR (KBr) ν/cm^{-1} 3448 (OH), 3362 (NH), 2929 (C−H), 1736 (NC═O), 1637 (HOC═O); ^{1}H NMR (500 MHz, DMSO-d_6) δ 13.50 (1H, s, ArO*H*), 8.94 (1H, d, J = 8.0, N*H*), 8.30−8.32 (1H, m, Ar-*H*), 8.26−8.28 (1H, m, Ar-*H*), 7.97−7.99 (2H, m, 2 × Ar-*H*), 7.26−7.27 (4H, m, 4 × Ph-*H*), 7.17−7.21 (1H, m, Ph-*H*), 4.79−4.83 (1H, m, C*H*), 3.27−3.32 (2H, m, PhC*H*$_2$); ^{13}C NMR (125 MHz, DMSO-d_6) δ 172.1 (C═O), 168.4 (*C*═O), 154.3 (Ar*C*), 138.5 (Ar*C*), 137.4 (Ph*C*), 131.8 (PhCH), 131.7 (PhCH), 129.5 (Ar*C*), 129.1 (2 × ArCH), 128.6 (ArC), 128.3 (2 × PhCH), 126.6 (PhCH), 126.1 (ArCH), 123.0 (ArCH), 120.3 (Ar*C*), 53.2 (*C*H), 35.9 (PhCH$_2$). HMRS calcd for $C_{19}H_{14}ClN_2O_4$ [M − H]$^-$ 369.0648; Found 369.0651. Anal. ($C_{19}H_{15}ClN_2O_4$) requires: C, 61.55; H, 4.08; N, 7.56%; found C, 61.61; H, 4.01; N, 7.62%.

■ ASSOCIATED CONTENT

Ⓢ Supporting Information

Details of synthesis, IC_{50} curves and crystallography. This material is available free of charge via the Internet at http://pubs.acs.org.

Accession Codes

The coordinates of crystal structures of FTO in complex with **1**, **2**, **3**, **6**, **11**, and **19** have been deposited in RCSB Protein Data Bank as PDB IDs 4IDZ, 4IE0, 4IE4, 4IE5, 4IE6, and 4IE7, respectively.

■ AUTHOR INFORMATION

Corresponding Author

*(M.A.McD.) Phone: +44(0)1865 275 629; E-mail: michael.mcdonough@chem.ox.ac.uk. (C.J.S.) Phone: +44(0)1865 275 625; E-mail: christopher.schofield@chem.ox.ac.uk

Present Address

[†]School of Chemical Sciences, Universiti Sains Malaysia, 11800 USM, Pulau Pinang, Malaysia.

Notes

The authors declare no competing financial interests.

■ ACKNOWLEDGMENTS

We thank the Biotechnological and Biological Sciences Research Council, and Pfizer (U.K.) for funding our NAOX work, as well as the Malaysian government and Universiti Sains Malaysia (scholarship for K.K.Y.) for financial support. We thank Jacob Bush, Marcus Sims, and Luc Henry for help with organic synthesis, Martin Münzel for advice on protein purification, Ian Clifton and Rasheduzzaman Chowdhury for advice on crystallography, Akane Kawamura and Richard Hopkinson for discussions, and the beamline staff at Diamond Light Source for assistance.

■ ABBREVIATIONS USED

FTO, fat mass and obesity associated protein; 2OG, 2-oxoglutarate; NAOX, nucleic acid oxygenase; ABH, AlkB human homologue; HIF, hypoxia-inducible transcription factor; JmjC, Jumonji C domain containing histone demethylase; DSF, dynamic scanning fluorometry; ΔT_m, melting temperature shift; LC, liquid chromatography; NOG, *N*-oxalylglycine; 3meT, 3-methylthymidine; 6meA, 6-methyladenosine; DSBH, double-stranded β helix; PHD, HIF-prolyl hydroxylase; TCA cycle, tricarboxylic acid cycle/Krebs cycle; IPTG, isopropyl β-D-1-thiogalactopyranoside; DMSO, dimethyl sulfoxide; MES, 2-(*N*-morpholino)ethanesulfonic acid; ESI-TOF, electrospray ionization time-of-flight

■ REFERENCES

(1) Frayling, T. M.; Timpson, N. J.; Weedon, M. N.; Zeggini, E.; Freathy, R. M.; Lindgren, C. M.; Perry, J. R.; Elliott, K. S.; Lango, H.; Rayner, N. W.; Shields, B.; Harries, L. W.; Barrett, J. C.; Ellard, S.; Groves, C. J.; Knight, B.; Patch, A. M.; Ness, A. R.; Ebrahim, S.; Lawlor, D. A.; Ring, S. M.; Ben-Shlomo, Y.; Jarvelin, M. R.; Sovio, U.; Bennett, A. J.; Melzer, D.; Ferrucci, L.; Loos, R. J.; Barroso, I.; Wareham, N. J.; Karpe, F.; Owen, K. R.; Cardon, L. R.; Walker, M.; Hitman, G. A.; Palmer, C. N.; Doney, A. S.; Morris, A. D.; Smith, G. D.; Hattersley, A. T.; McCarthy, M. I. A common variant in the *FTO* gene is associated with body mass index and predisposes to childhood and adult obesity. *Science* **2007**, *316*, 889−894.

(2) Church, C.; Lee, S.; Bagg, E. A.; McTaggart, J. S.; Deacon, R.; Gerken, T.; Lee, A.; Moir, L.; Mecinovic, J.; Quwailid, M. M.; Schofield, C. J.; Ashcroft, F. M.; Cox, R. D. A mouse model for the metabolic effects of the human fat mass and obesity associated *FTO* gene. *PLoS Genet.* **2009**, *5*, e1000599.

(3) Church, C.; Moir, L.; McMurray, F.; Girard, C.; Banks, G. T.; Teboul, L.; Wells, S.; Bruning, J. C.; Nolan, P. M.; Ashcroft, F. M.; Cox, R. D. Overexpression of FTO leads to increased food intake and results in obesity. *Nat. Genet.* **2010**, *42*, 1086−1092.

(4) Gerken, T.; Girard, C. A.; Tung, Y. C.; Webby, C. J.; Saudek, V.; Hewitson, K. S.; Yeo, G. S.; McDonough, M. A.; Cunliffe, S.; McNeill, L. A.; Galvanovskis, J.; Rorsman, P.; Robins, P.; Prieur, X.; Coll, A. P.; Ma, M.; Jovanovic, Z.; Farooqi, I. S.; Sedgwick, B.; Barroso, I.; Lindahl, T.; Ponting, C. P.; Ashcroft, F. M.; O'Rahilly, S.; Schofield, C. J. The obesity-associated FTO gene encodes a 2-oxoglutarate-dependent nucleic acid demethylase. *Science* **2007**, *318*, 1469−1472.

(5) Jia, G.; Yang, C. G.; Yang, S.; Jian, X.; Yi, C.; Zhou, Z.; He, C. Oxidative demethylation of 3-methylthymine and 3-methyluracil in single-stranded DNA and RNA by mouse and human FTO. *FEBS Lett.* **2008**, *582*, 3313−3319.

(6) Jia, G.; Fu, Y.; Zhao, X.; Dai, Q.; Zheng, G.; Yang, Y.; Yi, C.; Lindahl, T.; Pan, T.; Yang, Y. G.; He, C. N6-methyladenosine in nuclear RNA is a major substrate of the obesity-associated FTO. *Nat. Chem. Biol.* **2011**, *7*, 885−887.

(7) Thalhammer, A.; Aik, W.; Bagg, E. A. L.; Schofield, C. J. The potential of 2-oxoglutarate oxygenases acting on nucleic acids as therapeutic targets. *Drug Discovery Today Ther. Strateg.* **2012**, *9*, e91−e100.

(8) Fu, Y.; Dai, Q.; Zhang, W.; Ren, J.; Pan, T.; He, C. The AlkB domain of mammalian ABH8 catalyzes hydroxylation of 5-methoxycarbonylmethyluridine at the wobble position of tRNA. *Angew. Chem., Int. Ed.* **2010**, *49*, 8885−8888.

(9) Fu, Y.; He, C. Nucleic acid modifications with epigenetic significance. *Curr. Opin. Chem. Biol.* **2012**, *16*, 516−524.

(10) van den Born, E.; Vagbo, C. B.; Songe-Moller, L.; Leihne, V.; Lien, G. F.; Leszczynska, G.; Malkiewicz, A.; Krokan, H. E.; Kirpekar, F.; Klungland, A.; Falnes, P. O. ALKBH8-mediated formation of a novel diastereomeric pair of wobble nucleosides in mammalian tRNA. *Nat. Commun.* **2011**, *2*, 172.

(11) Rose, N. R.; McDonough, M. A.; King, O. N.; Kawamura, A.; Schofield, C. J. Inhibition of 2-oxoglutarate dependent oxygenases. *Chem. Soc. Rev.* **2011**, *40*, 4364−4397.

(12) Woon, E. C.; Demetriades, M.; Bagg, E. A.; Aik, W.; Krylova, S. M.; Ma, J. H.; Chan, M.; Walport, L. J.; Wegman, D. W.; Dack, K. N.; McDonough, M. A.; Krylov, S. N.; Schofield, C. J. Dynamic combinatorial mass spectrometry leads to inhibitors of a 2-oxoglutarate-dependent nucleic acid demethylase. *J. Med. Chem.* **2012**, *55*, 2173−2184.

(13) Han, Z.; Niu, T.; Chang, J.; Lei, X.; Zhao, M.; Wang, Q.; Cheng, W.; Wang, J.; Feng, Y.; Chai, J. Crystal structure of the FTO protein reveals basis for its substrate specificity. *Nature* **2010**, *464*, 1205−1209.

(14) King, O. N.; Li, X. S.; Sakurai, M.; Kawamura, A.; Rose, N. R.; Ng, S. S.; Quinn, A. M.; Rai, G.; Mott, B. T.; Beswick, P.; Klose, R. J.; Oppermann, U.; Jadhav, A.; Heightman, T. D.; Maloney, D. J.; Schofield, C. J.; Simeonov, A. Quantitative high-throughput screening identifies 8-hydroxyquinolines as cell-active histone demethylase inhibitors. *PLoS One* **2010**, *5*, e15535.

(15) Chowdhury, R.; Yeoh, K. K.; Tian, Y. M.; Hillringhaus, L.; Bagg, E. A.; Rose, N. R.; Leung, I. K.; Li, X. S.; Woon, E. C.; Yang, M.; McDonough, M. A.; King, O. N.; Clifton, I. J.; Klose, R. J.; Claridge, T. D.; Ratcliffe, P. J.; Schofield, C. J.; Kawamura, A. The oncometabolite 2-hydroxyglutarate inhibits histone lysine demethylases. *EMBO Rep.* **2011**, *12*, 463−469.

(16) Rose, N. R.; Ng, S. S.; Mecinovic, J.; Lienard, B. M.; Bello, S. H.; Sun, Z.; McDonough, M. A.; Oppermann, U.; Schofield, C. J. Inhibitor scaffolds for 2-oxoglutarate-dependent histone lysine demethylases. *J. Med. Chem.* **2008**, *51*, 7053−7056.

(17) Rotili, D.; Altun, M.; Kawamura, A.; Wolf, A.; Fischer, R.; Leung, I. K.; Mackeen, M. M.; Tian, Y. M.; Ratcliffe, P. J.; Mai, A.; Kessler, B. M.; Schofield, C. J. A photoreactive small-molecule probe for 2-oxoglutarate oxygenases. *Chem. Biol.* **2011**, *18*, 642−654.

(18) Demetriades, M.; Leung, I. K.; Chowdhury, R.; Chan, M. C.; McDonough, M. A.; Yeoh, K. K.; Tian, Y. M.; Claridge, T. D.; Ratcliffe, P. J.; Woon, E. C.; Schofield, C. J. Dynamic combinatorial chemistry employing boronic acids/boronate esters leads to potent oxygenase inhibitors. *Angew. Chem., Int. Ed.* **2012**, *51*, 6672−6675.

(19) Chen, B.; Ye, F.; Yu, L.; Jia, G.; Huang, X.; Zhang, X.; Peng, S.; Chen, K.; Wang, M.; Gong, S.; Zhang, R.; Yin, J.; Li, H.; Yang, Y.; Liu, H.; Zhang, J.; Zhang, H.; Zhang, A.; Jiang, H.; Luo, C.; Yang, C. G. Development of Cell-Active N(6)-Methyladenosine RNA Demethylase FTO Inhibitor. *J. Am. Chem. Soc.* **2012**, *134*, 17963−17971.

(20) Yan, L.; Colandrea, V. J.; Hale, J. J. Prolyl hydroxylase domain-containing protein inhibitors as stabilizers of hypoxia-inducible factor: small molecule-based therapeutics for anemia. *Expert Opin. Ther. Pat.* **2010**, *20*, 1219−1245.

(21) Arend, M. P.; Flippin, L. A.; Volkmar, G. P.; Ho, W. B.; Turtle, E. D.; Du, X. Novel nitrogen-containing heteroaryl compounds and methods of use thereof. WO 2004 108681 A1, 2004.

(22) Stubbs, C. J.; Loenarz, C.; Mecinovic, J.; Yeoh, K. K.; Hindley, N.; Lienard, B. M.; Sobott, F.; Schofield, C. J.; Flashman, E. Application of a proteolysis/mass spectrometry method for investigating the effects of inhibitors on hydroxylase structure. *J. Med. Chem.* **2009**, *52*, 2799−2805.
(23) Hausinger, R. P. FeII/alpha-ketoglutarate-dependent hydroxylases and related enzymes. *Crit. Rev. Biochem. Mol. Biol.* **2004**, *39*, 21−68.
(24) Frezza, C.; Pollard, P. J.; Gottlieb, E. Inborn and acquired metabolic defects in cancer. *J. Mol. Med. (Berlin)* **2011**, *89*, 213−220.
(25) Mole, D. R.; Schlemminger, I.; McNeill, L. A.; Hewitson, K. S.; Pugh, C. W.; Ratcliffe, P. J.; Schofield, C. J. 2-Oxoglutarate analogue inhibitors of HIF prolyl hydroxylase. *Bioorg. Med. Chem. Lett.* **2003**, *13*, 2677−2680.
(26) Elvidge, G. P.; Glenny, L.; Appelhoff, R. J.; Ratcliffe, P. J.; Ragoussis, J.; Gleadle, J. M. Concordant regulation of gene expression by hypoxia and 2-oxoglutarate-dependent dioxygenase inhibition: the role of HIF-1alpha, HIF-2alpha, and other pathways. *J. Biol. Chem.* **2006**, *281*, 15215−15226.
(27) Niesen, F. H.; Berglund, H.; Vedadi, M. The use of differential scanning fluorimetry to detect ligand interactions that promote protein stability. *Nat. Protoc.* **2007**, *2*, 2212−2221.
(28) Otwinowski, Z.; Minor, W. Processing of X-ray diffraction data collected in oscillation mode. *Method Enzymol.* **1997**, *276*, 307−326.
(29) McCoy, A. J.; Grosse-Kunstleve, R. W.; Adams, P. D.; Winn, M. D.; Storoni, L. C.; Read, R. J. Phaser crystallographic software. *J. Appl. Crystallogr.* **2007**, *40*, 658−674.
(30) Adams, P. D.; Afonine, P. V.; Bunkoczi, G.; Chen, V. B.; Davis, I. W.; Echols, N.; Headd, J. J.; Hung, L. W.; Kapral, G. J.; Grosse-Kunstleve, R. W.; McCoy, A. J.; Moriarty, N. W.; Oeffner, R.; Read, R. J.; Richardson, D. C.; Richardson, J. S.; Terwilliger, T. C.; Zwart, P. H. PHENIX: a comprehensive Python-based system for macromolecular structure solution. *Acta Crystallogr. D* **2010**, *66*, 213−221.
(31) Emsley, P.; Lohkamp, B.; Scott, W. G.; Cowtan, K. Features and development of Coot. *Acta Crystallogr. D* **2010**, *66*, 486−501.
(32) Balzarini, J.; Celen, S.; Karlsson, A.; de Groot, T.; Verbruggen, A.; Bormans, G. The effect of a methyl or 2-fluoroethyl substituent at the N-3 position of thymidine, 3′-fluoro-3′-deoxythymidine and 1-beta-D-arabinosylthymine on their antiviral and cytostatic activity in cell culture. *Antivir. Chem. Chemother.* **2006**, *17*, 17−23.